Civil and Environmental Engineering
Vol. 21, Issue 1, 437-461, DOI: 10.2478/cee-2025-0034

PERFORMANCE EVALUATION OF CIRCULAR CYLINDRICAL SHELLS UNDER COMBINED AXIAL COMPRESSION AND TORSION

Mustafa Ayad MURAD[1, 2, *], Hossein SHOWKATI[2]

[1] Department of Civil Engineering, College of Engineering, Al-Iraqia University, Baghdad, Iraq
[2] Department of Civil Engineering, College of Engineering, Urmia University, Urmia, Iran
[*] corresponding author: mustafa.a.murad@uoaliraqia.edu.iq

Abstract

Cylindrical shells, prevalent across diverse industries, often encounter combined loading, including axial compression and torsion. Buckling poses a major threat to their structural integrity. This study proposes Carbon Fiber Reinforced Polymer (CFRP) as an innovative strengthening method for steel cylindrical shells subjected to combined loading. The main objective was to explore how CFRP strengthening influences the buckling behavior of steel shells and to evaluate the effects of various parameters such as thickness, stacking sequence, and imperfections. The research methodology involved three steps. First, model validation was achieved using experimental data and established theories from CFRP and steel cylindrical shell specimens. Then, three types of FE models were created: a steel shell, a CFRP shell, and a CFRP-strengthened steel shell, all with identical dimensions. These models underwent combined loading with continuous load and deformation measurements. Sensitivity analyses were subsequently conducted to evaluate the influence of geometry, material properties, and initial imperfections on buckling performance. The results indicated that increasing shell thickness significantly improves performance by boosting stiffness and load capacity, but at the cost of greater axial shortening. CFRP reinforcement offers similar benefits, with effectiveness depending on the specific implementation strategy. Conversely, axisymmetric imperfections have a detrimental effect, slightly reducing stiffness and load capacity. Finally, the sensitivity of various performance parameters is highly dependent on the design choices and specific model being analyzed. These findings provide valuable insights for steel cylindrical shell design in various engineering applications.

Keywords:

Cylindrical Shell;
CFRP;
Axial compression;
Torsion;
Buckling.

1 Introduction

Cylindrical shells, widely employed in diverse applications like aircraft, missiles, boilers, pipelines, automobiles, and submarine structures, are favored for their simple geometry and ease of manufacture [1]. Extensive research has been dedicated to understanding and optimizing this prevalent thin-shell structure [2]. Buckling in these structures, especially under axial compression, leads to large deformations perpendicular to the loading direction, causing a significant loss of load-carrying capability [3]. They often face diverse loadings, including axial compression, bending, torsion, and combinations thereof, making understanding their failure behavior crucial. Thinner cylinders, prevalent in aerospace applications, primarily fail due to elastic buckling, while thicker cylinders, common in marine and offshore applications, experience plastic buckling as the dominant failure mode [2]. They are often subjected to combined loadings of axial compression, circumferential compression, shear and torsion [4]. Torsional buckling, regarded as a critical failure mode in thin-walled structures, has been extensively studied over the decades [5]. Researchers, including Ekstrom in 1963, Yamaki in 1976, Yamaki and Matsuda in 1976, and subsequent studies by De-yu et al. in 1992, Louca and Harding in 1994, Tan in 2000, Sofiyev in 2003, Zhang and Tong in 2004, Xu et al. in 2010, 2013, Ninh et al. in 2015, Shakouri et al. in 2017, and Cho in 2018, have contributed significantly to understanding torsional buckling behaviors in cylindrical shells [6-18]. There are also various research studies which have concentrated on developing optimal composite shells to improve strength under diverse loading conditions. These conditions include pure axial compression [19–24], combined axial compression and torsion [25–27], transverse load [28], combined axial compression and pressure [29 and 30], and combined axial compression, bending, and pressure [31]. These studies encompass experimental, theoretical, and analytical approaches, revealing critical insights into the diverse behaviors of cylindrical shells under different loads [5]. However, the existing studies focuses more on traditional stiffening methods and there is also limited information available regarding the buckling behavior of strengthened cylindrical shells under combined loading [4]. Unlike columns or flat plates, thin cylindrical shells exhibit complex behavior, with an unstable post-buckling phase where the load drops abruptly after reaching critical strength [2]. Various techniques have been explored for strengthening cylindrical shells against buckling, with ring stiffeners and stringers being commonly used methods [32]. However, these methods have some deficiencies and new strengthening method must be proposed and employed. For steel cylindrical shells, the confinement method using fiber-reinforced polymers (FRP) emerges as an effective strategy. FRP, a composite material comprising fibers and resin, gains strength from the fibers while the resin binds them together. The fibers, made from carbon, aramid, or glass, offer variable strength based on their composition [33]. External wrapping of metallic cylindrical shells with one or more layers of FRP composite enhances their buckling performance [34]. While there's extensive research on strengthening metal shells against buckling, the use of CFRP for enhancing the buckling strength of thin metallic shells remains largely unexplored [32]. The concept of using CFRP in repairing and reinforcing steel or concrete shells is a relatively new area in literature. Current studies often focus on localized reinforcement, like patches inhibiting fatigue cracks or addressing specific defects. However, there's a gap in quantitative studies on the buckling behavior of metal shells strengthened with CFRP, considering both experimental and numerical approaches [35].

The utilization of CFRP composite materials for reinforcing cylindrical shells represents inherent advantages such as corrosion resistance, lightweight properties, high tensile strength, stiffness, and malleability for desired configurations, CFRP presents a promising avenue for shell reinforcement. Despite these merits, there exists limited research on the buckling behavior of cylindrical shells strengthened with CFRP, particularly under combined loading scenarios such as axial compression and torsion [36]. Traditional techniques exhibit deficiencies, and environmental impacts associated with FRP require careful consideration [36]. In light of this, a comprehensive review of prior research on the topic becomes imperative to identify existing research gaps, formulate hypotheses, and pinpoint potential innovations guiding the current investigation.

Beginning with Bisagni's exploration of carbon-epoxy laminated cylindrical shells subjected to axial compression and torsion in 1998, subsequent studies have continued to broaden the knowledge base [37]. Tafreshi and Bailey's study in 2007 investigated the instability of imperfect composite cylindrical shells, shedding light on challenges posed by imperfections [4]. The research community further explored the application of fiber-reinforced polymers (FRP) in enhancing structural performance, with studies by Teng and Hu in 2007 on FRP-jacketed circular steel tubes and Batikha's 2008 focus on the strengthening of thin metallic cylindrical shells using FRP [33 and 32]. Addressing diverse loading scenarios, Shariati et al. (2012) and Allahbakhsh and Shariati (2014) studied the ratcheting characteristics of cylindrical shells under cyclic axial loading and the instability of cracked CFRP composite cylindrical shells under combined loading, respectively [1 and 31]. Ifayefunmi's 2016 comprehensive investigation into the buckling behavior of axially compressed cylindrical shells provided a comparative analysis between theoretical predictions and experimental data [2]. Exploring the inelastic buckling of functionally graded material (FGM) cylindrical shells subjected to combined axial and torsional loads, Huang et al. in 2017 expanded the understanding of material behavior [38]. Draidi et al.'s 2018 study focused on the buckling behavior of metallic cylindrical shell structures strengthened with CFRP composites, contributing insights into hybrid material systems [35]. The scope of research extended to include instability under bending conditions, as demonstrated by Yadav and Gerasimidis in 2019 [39]. Fan's study in 2019 introduced a novel approach for predicting critical buckling loads of axially compressed cylindrical shells using non-destructive probing methods, offering innovative insights into predictive methodologies [40]. Advancements in probabilistic and deterministic lower-bound design benchmarks for cylindrical shells under axial compression were presented by Wagner et al. in 2020 [41]. Additionally, Wagner et al. explored buckling with loading imperfections, conducting an experimental and numerical campaign on low knockdown factors [3]. The exploration of hybrid materials continued with Krishna et al. in 2020, conducting a modeling study on the buckling characteristics of metal-FRP hybrid cylinders [42]. Shahgholian-Ghahfarokhi et al.'s 2021 study conducted torsional buckling analyses on functionally graded porous Nano-composite cylindrical shells reinforced with grapheme platelets, contributing to the emerging field of advanced materials [5]. Taraghi et al. in 2021 conducted a parametric study on the buckling stability of CFRP-strengthened cylindrical shells subjected to uniform external pressure, addressing practical considerations in the application of strengthening techniques [36]. As the literature unfolds, Krishna et al. in 2021 evaluated the effectiveness of FRP strengthening on the buckling characteristics of metallic cylindrical shells which adds valuable insights into the performance of hybrid materials [34].

Researchers have significantly advanced the understanding of imperfections, retrofitting techniques, and material characteristics in cylindrical shell structures. Previous works have explored applications of fiber-reinforced polymers (FRP), hybrid material systems, and advanced materials like functionally graded porous, nano composites reinforced with grapheme platelets. These studies have introduced approaches, including predictive methodologies, non-destructive probing methods, and advancements in probabilistic and deterministic design benchmarks. The current study builds upon this foundation, introducing several innovations in the analysis of cylindrical shell structures subjected to combined axial compression and torsion through advanced numerical modeling techniques. This research explores a novel application of CFRP for enhancing the buckling strength of thin metallic shells, particularly steel cylindrical shells. The study also investigates the effectiveness of CFRP strengthening under combined loading conditions of axial compression and torsion. The inclusion of sensitivity analyses in the research design is another innovative approach in which the effect of factors like geometry variations, material properties, and initial imperfections will be investigated on the buckling behavior of CFRP-strengthened steel cylindrical shells. The findings from this study can be used to improve the design and maintenance practices of cylindrical shells in various industries, such as construction, aerospace, and transportation. The research also contributes to the development of efficient and sustainable strengthening techniques for cylindrical shells.

2 Methodology

A three-step numerical approach will be employed to precisely analyze the buckling behavior of cylindrical shells under combined axial compression and torsion. This methodology adheres to a rigorous scientific approach that involves reproducing a reference model, verifying the modeling procedure and its results, and finally, progressing the research by incorporating innovations. The first step involves validation. Here, an experimental CFRP cylindrical shell specimen from Meyer-Piening et al. (2001) serves as our reference model [27]. Their experimental data will be used to validate the finite element (FE) modeling procedure created within ABAQUS software for CFRP cylindrical shells. To ensure the software's accuracy, an additional steel cylindrical shell model will be verified using established theoretical equations. Following validation, the second step focuses on model development. Three cylindrical models with identical dimensions will be created: one made of steel, another of CFRP, and a third combining steel strengthened with CFRP. The final step involves buckling analysis and sensitivity studies. The models will be subjected to combined axial compression and torsion loading, while load and deformation measurements are continuously recorded. Sensitivity analyses will then be performed to assess how the buckling performance of the cylindrical shells under combined loading is affected by variations in geometry, material properties, and the presence of initial geometric imperfections. The results will be analyzed comprehensively to understand how each of these factors influences buckling behavior. Furthermore, the effectiveness of CFRP strengthening in improving the buckling resistance of steel shells will be evaluated.

2.1 Reference models

Two reference models were considered for this study, the first one is an experimental specimen of CFRP cylindrical shell and the second one is a steel cylindrical shell with the same geometry. For the CFRP model, sample Z30 from Meyer-Piening et al. research work was selected as it was also adopted by Tafreshi and Bailey in 2007. They studied thin-walled, circular cylindrical shells made from carbon fiber laminates with varying orientations. The shells had a common length of 510 millimeters and a diameter of 500 millimeters. They were made of 10 layers, each 0.125 millimeters thick. As a result, the nominal wall thickness of all the samples was 1.25 millimeters. Table 1 shows the geometry of the cylindrical shell studied by Meyer-Piening et al. [27].

Table 1: Geometry of the cylindrical shell [27].

L [mm]	d [mm]	R [mm]	t [mm]	L/R	r/R	ply thickness [mm]
510	500	250	1.25	2.04	200	0.125

The researchers chose specific layer configurations to achieve a wide range of axial buckling loads. The shell samples were made from carbon fiber epoxy prepregs. These prepregs were produced by winding filaments over a heated cylindrical mold. The prepregs were then cut into specific sizes and layered around a steel cylinder. The 0° layer represents the axial direction of the shell, while the +45° layer is tilted upwards to the right when viewed from the outside. After each layer was applied, a rubber roller was used to remove any gaps between the fibers and any air bubbles. A tear-off fabric was then added, followed by a layer of tensioned glass fibers. The laminate was then cured at 140°C for 12 hours. Once cured, the glass fiber layer and the core were removed, and the shells were trimmed so that the edges were perpendicular to the cylinder's axis. At this point, each sample was 530 millimeters long. Furthermore, the circular cylinder characterized by its diameter *D*, radius *R*, and uniform wall thickness *t*, and an axial length L. Fig. 1 shows the test specimen and schematic view of the geometry of the samples [27].

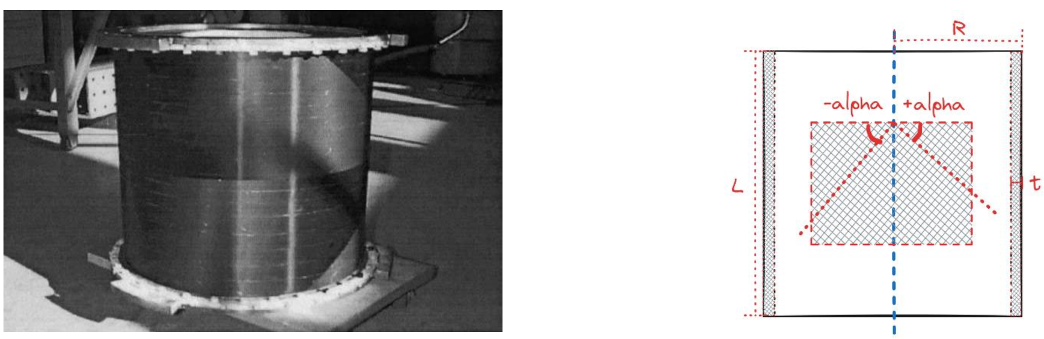

experimental specimen of CFRP | layer configuration

Fig. 1: Test specimen and schematic view of the geometry of Z30 [27].

The stacking sequence was ±53, ±38, ±22, ±90 and ±30 in which the first numbers indicate the outside layer. The boundary condition of the specimen was rigidly built-in edges. The stiffness properties of the shells were computed using lamination theory, which takes into account the material stiffness of the individual layers. The material properties themselves were determined based on a large number of coupon tests. Based on the results, the experimental and numerical buckling load for Z30 were 282.52 and 276 kN for axial load respectively and 17.4 kNm for both approaches under torsion. Table 2 presents the engineering constants for CFRP reported by Meyer-Piening et al. and Tafreshi and Bailey to further study the models using finite element method [27].

Table 2: Engineering constants for the CFRP used by Meyer-Piening et al. and Tafreshi and Bailey [4, 27].

Material no.	E_L/E_T	m_{LT}	G_{LT}/E_T	G_{TT}/G_{LT}	E_T [GPa]
Carbon fiber reinforced polymer (CFRP)	14.18	0.31	0.654	1.0	8.70

In this study, it was decided to model the steel cylindrical shell based on the geometry of the CFRP model while the material of the steel was adopted from the study of Taraghi et al. The procedure of the FE modeling of both reference models are almost identical. However, the buckling results of the steel cylindrical shell under axial compression and torsion will be verified using theoretical equations.

2.2 Finite Element Analyses

The finite element analysis (FEA) software used in this study is ABAQUS. This specific software was chosen because it is well-suited for analyzing nonlinear material behavior and geometric nonlinearities, which are important factors in modeling the buckling of shells. The modeling procedure adopted here was similar to Tafreshi and Bailey study, ensuring robustness even under steep deformation gradients and asymmetric buckles. The shells themselves were modeled using four-node bilinear shell elements. These elements are a good choice for this application because they are computationally efficient and can accurately capture the bending behavior of thin shells. For the CFRP model, the geometric dimensions and material properties were chosen to match those of the real shells that were tested by Meyer-Piening et al. Table 3 presents the material property of the CFRP calculated based on Table 2, according to lamination theory using material stiffness, and introduced as unidirectional orthotropic lamina in ABAQUS. Then, the layup of CFRP based on the stacking sequence of Z30 composed of 10 plies with their thickness and orientation angles were defined and assigned to the model (Fig. 2). In this procedure, a local coordination system was also assigned to the CFRP layup. Based on this, the CFRP sheet was considered orthotropic with two Young's moduli in circumferential and meridional directions, along with a Poisson's ratio. The coordinate axes (x, y, z) corresponded to axial, circumferential, and inward normal directions.

Table 3: Material property of the CFRP used in ABAQUS.

Material	v_{12}	E_2 [Mpa]	E_1 [Mpa]	G_{12} [Mpa]	G_{13} [Mpa]	G_{23}
CFRP	0.31946	8707.9	123550	5695	5689.8	3400

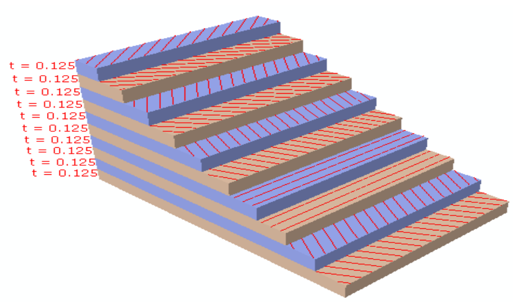

Fig. 2: Stacking sequence for CFRP introduced in ABAQUS.

To simplify boundary condition application and loading, the top and bottom ends of the models were constrained to maintain their flat, circular shapes throughout the simulation. This involved coupling the nodes at these ends to reference points. Both ends of the model were fixed in all directions except for the top end, which was allowed free axial movement. This configuration enables the application of axial loads while constraining other motions. For the torsional buckling analysis, the top end was granted free rotation about the longitudinal axis only. All other degrees of freedom were fixed. In the case of combined axial compression and torsion, both the axial displacement and rotational freedom around the longitudinal axis were permitted at the top end [4]. Using a fix support for the cylindrical shell ends in the model led to much better agreement with the actual test results and no initial small deflection was applied [33]. Concentrated compressive force (F) was applied at the reference point assigned to the top end of CFRP cylindrical shell to simulate axial load, and pure torsional moment (T) were introduced using moment load in ABAQUS, ensuring nodes on each end cross-section remained on the same planes during deformation. The specimen was modeled employing four-node, three-dimensional doubly curved shell elements with six degrees of freedom (S4R). The S4R element offers a practical balance of computational efficiency and accuracy, as demonstrated by verification results. While the S8R element could provide finer meshing, it would increase computational costs without substantial gains in accuracy for this specific application. Moreover, the S4R element is widely adopted for thin to moderately thick shells, as evidenced by Krishna et al.'s study [41], and has proven robust under combined loading conditions. The S4R element was found to adequately capture the necessary behavior in our simulations. The element size as recommended by Meyer-Piening et al. was chosen to be on the order of $0.5\times\sqrt{R\times t}$, where R is the radius and t is the thickness of the shell. A total of 11100 shell elements were used [27]. Fig. shows the boundary conditions and meshing of the CFRP cylindrical shell.

Fig. 3: Boundary conditions and meshing of the CFRP cylindrical shell.

The modeling approach for the steel cylindrical shell mirrored that of the CFRP model, with the sole exception of material properties. Steel was defined as an elastic-perfectly plastic material in ABAQUS, with details provided in

Table 4 and Fig..

Table 4: Material property of steel used in ABAQUS [36].

Material	E [Mpa]	ν	σ_y [Mpa]	ε_y	σ_u [Mpa]	ε_u
Steel	190800	0.3	205.48	0	332.16	0.02215

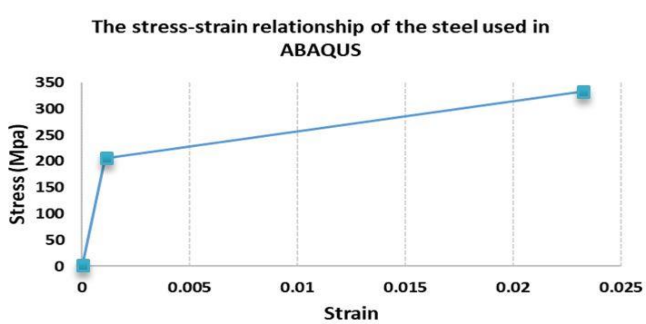

Fig. 4: Bilinear curve of steel introduced to ABAQUS.

Two different analyses that are linear eigenvalue buckling and nonlinear buckling using Riks method were performed for both CFRP and steel models. The Riks method, implemented in ABAQUS, was chosen for addressing unstable phases of the response during static equilibrium states. This method involves dynamic modeling of the response, including inertia effects, by restarting the static procedure and transitioning to a dynamic procedure when instability occurs. The Riks method was preferred over alternative approaches due to its effectiveness in global buckling and post buckling analyses. Note that both reference models were assumed to be geometrically perfect at the reproduction step.

2.3 Modeling Validation

The purpose of this section is to compare the buckling behavior of CFRP and steel shells with the experimental data and theoretical equations to validate the FE modeling process. For the CFRP model, the experimental data of Meyer-Peiening et al. research on CFRP composite cylindrical shells under combined axial and torsional loading was used. Fig. shows the interactive buckling curves for the CFRP shell configuration (L/R = 2.04 and R/t = 200) with the stacking sequence of [±53, ±38, ±22, ±90 and ±30]. These curves represent the relationship between axial and torsional loads at the point of buckling. As it can be seen, the trends observed in two approaches are similar and the ABAQUS results from this study have 2.72 and 3.15 percentage difference for torsional and axial buckling load compared to the experimental data of Meyer-Piening et al respectively. Fig. also represents first buckling mode of the CFRP cylindrical shell subjected to both axial compression and torsional moment.

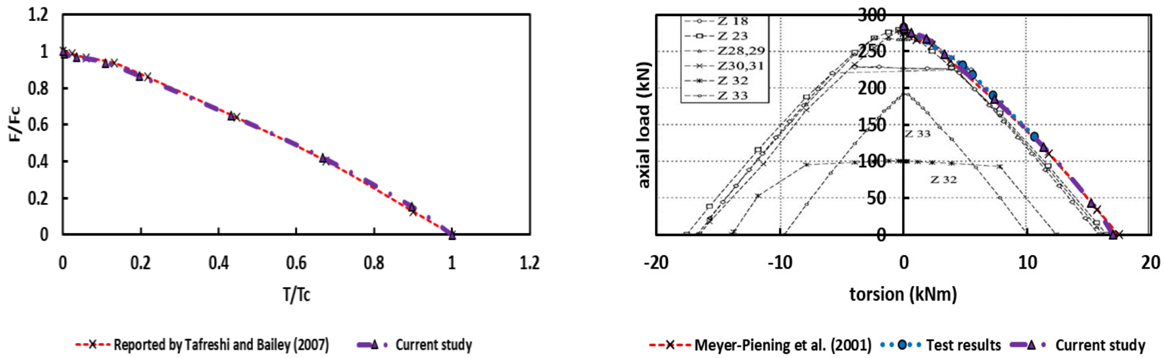

Fig. 5: Interaction buckling curve for a CFRP cylindrical shell subjected to both axial compression and torsional moment.

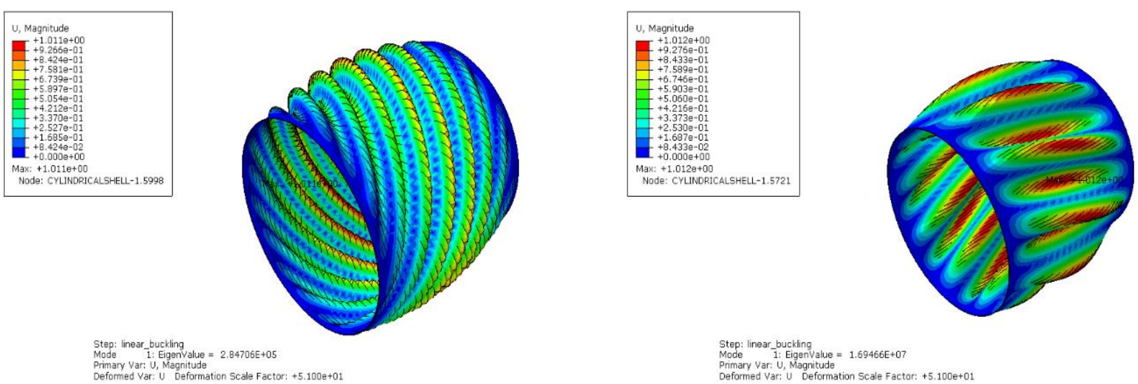

Fig. 6: First buckling mode of the CFRP cylindrical shell subjected to both axial compression and torsional moment.

To validate the modeling procedure of steel cylindrical shell in ABAQUS, the axial and torsional buckling result of this model was verified using established theoretical equations. The classical analysis of cylinder buckling relies on the assumption of a pre-buckling state, where bending stresses are disregarded, following Donnell shallow shell theory. Under this hypothesis, the elastic critical buckling load for an axially compressed cylinder with an axisymmetric mode is determined by the formula [5]:

$$F_{cyl} = \frac{2\pi E t^2}{\sqrt{3(1-v^2)}} \tag{1}$$

However, for relatively thick cylinders that undergo failure within the plastic region, the reference buckling load (F_{ref}) is defined as the load required to cause yielding, expressed as [5]:

$$F_{ref} = \pi D t \sigma_{yp} \tag{2}$$

Here, F_{cyl} represents the cylinder's classical elastic critical buckling load, F_{ref} denotes the cylinder's reference buckling load required to induce yielding, E stands for the Young's Modulus of the material, σ_{yp} is the yield stress of the material, v signifies the Poisson's ratio of the material, D represents the diameter of the cylinder, and t is the wall thickness of the cylinder [5].

To verify the critical buckling torque obtained for the steel cylindrical shell under torsion, Donnell's equation is utilized. This equation, specifically designed for moderately long, isotropic cylindrical shells, provides an estimate of the critical buckling torque [5]. The equation is expressed as:

$$T_{cr} = 2\pi R^2 t\tau \tag{3}$$

Herein, R is the radius of the cylindrical shell and t is the thickness of it. τ is calculated using following equation [5].

$$\tau = \frac{E}{1-\nu^2}\left(\frac{t}{L}\right)^2\left(4.6+\sqrt{7.8+1.67H^{\frac{3}{2}}}\right) \tag{4}$$

Where, L is the length of the cylindrical shell, v is Poisson's ratio and E is the modulus of elasticity. H is also obtained by [5]:

$$H = \frac{L^2\sqrt{1-\nu^2}}{2tR} \tag{5}$$

Table 5 shows the results of a buckling analysis of a steel cylindrical shell performed using ABAQUS finite element software and theoretical equations for both axial and torsional buckling. It is worth mentioning that F_{ref} was obtained 403.46 kN.

Table 5: Comparison of buckling loads for steel cylindrical shell (ABAQUS vs. Theory).

Fcr [kN]			**Tcr [kN]**		
ABAQUS	theoretical	Dif (%)	ABAQUS	theoretical	Dif (%)
1175.99	1133.70	3.73	70.56	73.93	4.56

Table 5 shows that the critical buckling loads predicted by ABAQUS are close to the theoretical values. The percentage difference is 3.73 percent for axial buckling and 4.56 percent for torsional buckling. This good agreement between the ABAQUS and theoretical results suggests that the FE modeling procedure used for the steel cylindrical shell is valid. Fig. 1 also shows the first buckling mode of the steel cylindrical shell subjected to both axial compression and torsional moment.

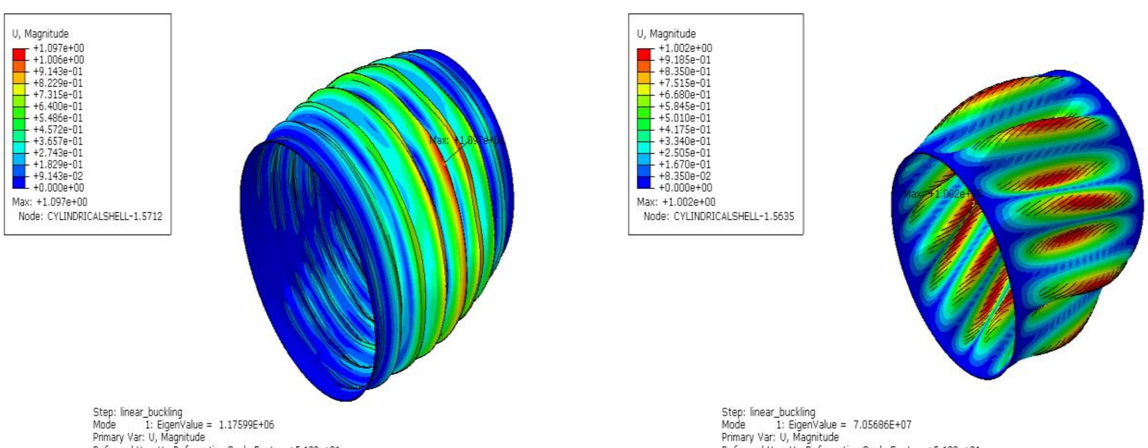

Fig. 7: First buckling mode of the steel cylindrical shell subjected to both axial compression and torsional moment.

2.4 Model development

In this study, after verifying the FE modeling procedure in ABAQUS, three types of cylindrical samples will be investigated to understand their buckling behavior under combined axial compression and torsion. The first two samples are the verified steel and CFRP cylindrical shells while the third one is the steel cylindrical shell strengthened by CFRP. All samples share common dimensions and for the steel sample strengthened by CFRP, it is assumed that CFRP layers will be externally bonded to the steel cylindrical shell using epoxy resin. Building upon the verified model from the previous sections, the FE modeling procedure for steel, CFRP, and steel cylindrical shell strengthened by CFRP introduces some key refinements for this section. In this step, both geometric and material behavior complexities are considered in the simulations to reflect real-world condition. For the strengthened sample, the steel shell and CFRP wrap are modeled as separate shell surfaces and tied to each other. Based on the study of Draidi et al., perfect adhesion between the CFRP layers is assumed. Through their tests, it has been determined that the bonding between steel and composite such as CFRP is not crucial in terms of bearing capacity [35]. In this study, perfect adhesion between steel and CFRP is assumed to simplify the analysis and focus on the primary behavior of the composite system. If no adhesion were considered instead, another constitutive model must be employed in ABAQUS to simulate debonding, potentially leading to a reduction in load transfer, altered stiffness, and different failure mechanisms as well as increasing the computational time and cost. No adhesive interactions could introduce slip or separation at the interface, affecting the structure's overall performance under load. Each CFRP layer is modeled as a distinct ply within the composite layup definition. Three integration points are used through the thickness of each CFRP layer, while five are used for the steel shell element. The composite layup includes specifications for shell thickness, material models, orientation, and integration points. The metallic shell uses the bi-linear isotropic elastic perfectly plastic model, while the CFRP employs the lamina constitutive model. ABAQUS provides two time integration approaches for this study: explicit and implicit algorithms. Implicit method solves a system of equations iteratively at each load increment using Newton-Raphson's method while it can become computationally expensive and lead to convergence issues. However, explicit algorithms directly advance the solution from the previous time step without iteration. They offer conditional stability and require a large number of small-time increments. Furthermore, in case of using eigenvalue buckling and the nonlinear RIKS method, this combination allows for capturing the initial buckling behavior and the subsequent post-buckling response, mimicking a slow buckling test. In contrast, the explicit solver facilitates the inclusion of dynamic effects, making it suitable for simulating rapid buckling scenarios. Due to the presence of material nonlinearities, the explicit solver is suggested for its ability to handle these complexities efficiently. This analysis method needs mass scaling and smooth loading application. The first one is used to further reduce the number of time increments. Artificially increasing the density of elements by a factor of 25 decreases the wave speed and allows for larger stable time increments. A displacement-controlled loading rate of 100 mm/s with a smooth step amplitude curve is used to minimize sudden changes in acceleration and avoid noisy solutions. However, increasing loading rates and mass scaling can introduce deviations from the true static solution due to inertial effects. To ensure results remain close to the quasi-static conditions observed in experiments, the kinetic energy is monitored and kept below 0.1 percent of the internal energy throughout the loading process. Double precision is employed throughout the analysis to minimize numerical errors associated with the large number of increments used in the explicit solver [42]. Table 6 and Fig. represent the results of using 5 different solvers which are Eigen solver, static general, RIKS, dynamic implicit, and quasi-dynamic explicit to study the buckling performance of the reference steel cylindrical shell strengthened by CFRP under combined axial compression and torsion.

Table 6: comparison of buckling loads from different solvers.

Analysis	F_{cr} [kN]	Dif [%]	Time of analysis [sec]	Dif [%]
Meyer-Piening et al. (2001)	282.53	NA	NA	NA
EigenSolver	284.70	0.77	103.00	NA
Static General	287.83	1.88	570.00	453.40
RIKS	288.88	2.25	426.00	313.59
Dynamic Implicit	270.17	-4.38	1603.00	1456.31
Quasi-dynamic explicit	295.64	4.64	23	-77.67

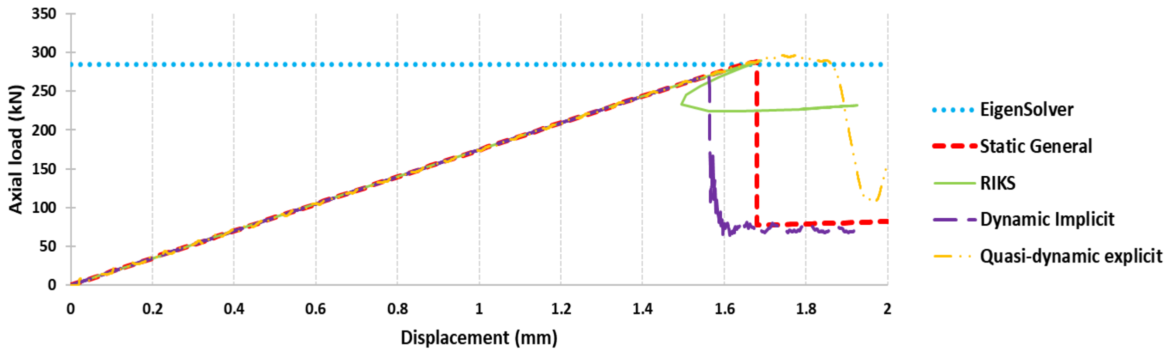

Fig. 8: Solution convergence characteristics of solvers for buckling analysis of CFRP-strengthened steel shell.

As it can be seen in Table 6 and Fig., the critical buckling load (F_{cr}), and time taken for analysis from each solver are compared while the reference value (282.53 kN) is taken from the work of Meyer-Piening et al. (2001). The results show that all solvers except Dynamic Implicit were able to predict the critical buckling load of the CFRP-strengthened steel shell with reasonable accuracy. The Eigen Solver, Static General, and RIKS solvers exhibited slight overestimations, while the Quasi-dynamic Explicit solver produced a small overestimation. The quasi-dynamic Explicit solver resulted in the highest critical buckling load (295.64 kN) among all solvers, representing a difference of 4.64 percent compared to the reference value while it took only 23 second (77.67 percent faster than Eigen Solver). Since it's important to consider the computational efficiency alongside accuracy, the Quasi-dynamic Explicit solver is selected for the rest of the analysis. This solver provides a good balance between accuracy and speed.

Following the selection of the most suitable solver, and based on the remaining modeling assumptions, clamped boundary conditions were applied to the bottom end of all samples. This translates to all degrees of freedom being restrained, preventing any rotations or displacements in any direction. Conversely, the top end allows for rotation around the longitudinal axis and axial displacement along the same axis. This enables the application of torsional and axial compression loads. The shell undergoes axial compressive concentrated force (F) and torsional moment (M) simultaneously. Both axial compression and torsion are applied in combination to investigate the buckling behavior under various loading conditions. Additionally, realistic imperfections measured on the inner surface of the models were incorporated to improve the accuracy of the simulations which will be describes in 3.3.3. Linear, quadrilateral shell elements (S4R) with finite membrane strain and reduced integration are chosen for all models. These elements are known for their robustness and ability to handle problems with steep deformation gradients, such as the axisymmetric bulge region observed in this study. Data collected from the analysis will be used to generate load-deformation curves, enabling the identification of critical points such as the onset of buckling, peak loads, axial and torsional stiffness, and failure points. Comparative analysis will then be conducted to highlight any differences in the buckling behavior among the steel, CFRP, and steel strengthened by CFRP samples. Throughout the analysis, load and deformation measurements will be continuously recorded. The objective is to observe and analyze the behavior of each sample type under the specified sensitivity analyses.

2.4.1 Sensitivity analysis on Geometry Variation

To effectively design CFRP strengthening for improved axial and torsional load capacity, a thorough understanding of buckling behavior and modes in cylindrical shells is crucial. This study investigates models with varying radius-to-thickness ratios (R/t) as detailed in Table 7 to capture a wide range of potential buckling modes and assess the impact of CFRP strengthening. While the diameter (D) and length (L) remain constant across all models, different r/t ratios are achieved by adjusting the shell thickness. To ensure consistent buckling behavior across the models, their configurations were chosen to have a medium length ($L/\lambda > 2$) which can be calculated using Eq. (6). This medium length eliminates the influence of length and boundary conditions on the buckling response [34]. Table 7 presents details of samples used for geometry sensitivity analysis.

$$\lambda = \frac{\pi}{\sqrt[4]{3(1-v^2)}}\sqrt{rt} \quad (6)$$

Table 7: Details of samples used for geometry sensitivity analysis.

Model nomenclature	Model diameter, D [mm]	Length [mm]	Thickness, t [mm]	R/t	L/λ
G1	500	510	1.25	200	11.8
G2	500	510	0.625	400	16.7
G3	500	510	2.5	100	8.35

2.4.2 Material sensitivity analyses

This section explores the influence of material properties on the buckling behavior of the models through two separate sensitivity analyses. The first analysis investigates the impact of varying laminate stacking sequences. These sequences are adopted from the work of Wagner et al. [3]. The second analysis focuses on the effect of the CFRP's transverse modulus. Here, three distinct values are examined by increasing and decreasing the primary transverse modulus (E_2) by 50 percent. This approach aligns with the findings of Krishna et al. [41], who observed a high sensitivity of buckling response in CFRP-strengthened cylindrical shells to variations in the transverse modulus. Table 8 presents the details of samples used for material sensitivity analysis.

Table 8: Details of samples used for material sensitivity analysis.

Model nomenclature	Model diameter, D [mm]	Length [mm]	Thickness, t [mm]	Stacking sequence	E_2 [Mpa]
Mss1	500	510	1.25	[±75, ±75]	8707.9
Mss2	500	510	1.25	[±51, ±90, ±90, ±40]	8707.9
Mss3	500	510	1.25	[±60, 0_2, ±68, ±52 and ±37]	8707.9
Mtm1	500	510	1.25	[±53, ±38, ±22, ±90 and ±30]	4353.95
Mtm2	500	510	1.25	[±53, ±38, ±22, ±90 and ±30]	17415.8

2.4.3 Effect of Initial Geometric Imperfection

Thin-walled structures are particularly susceptible to various buckling instabilities such as loading or geometric imperfections. Studying the buckling performance of cylindrical shell under geometric imperfections are common as geometric imperfections, characterized as deviations from the ideal structural shape, have the potential to substantially diminish the buckling load of thin-walled shells [3]. Initial imperfections are introduced on the shell surface to account for factors such as fabrication tolerances, weld depressions, and lap joints [42]. Moreover, this initial configuration can change over time, leading to a loss of conservatism in the initial design. During operation, new shape defects can arise due to accidental overloads or creep [35]. While shells undergoing elastic buckling are highly sensitive to imperfections, the chosen tube, relatively thick for its diameter, tends to fail through axisymmetric bulging near the tube end, resembling inelastic buckling [42]. In other words, in a perfect scenario with a flawless cylindrical shell under axial compression, both ends would develop "elephant's foot" buckles (local outward bulges). However, real-world complexities like minor irregularities in shape and material properties prevent this from happening. To account for such behavior, the finite element modeling must incorporate a deliberate geometric imperfection. This small imperfection had minimal impact on the overall load-deformation behavior but was sufficient to guide the simulated cylindrical shell into developing a single local buckle at one end, similar to what happens in real experiments [33].

In this study, an axisymmetric outward imperfection is introduced in the form of a half-wave sine curve, with its half-wavelength (a) determined by Eq. (7), representing the longitudinal half-wavelength of the classical axisymmetric elastic buckling mode of axially compressed cylinders. This imperfection, centered at the position of maximum radial displacement obtained from linear elastic FE analysis near the shell end. In CFRP strengthened shell, to address the possibility of asymmetric buckling away from ends due to restraining of axisymmetric bulging near the tube ends, an imperfection (w) described in Eq. (8) is employed. This imperfection combines axisymmetric and asymmetric buckling, featuring continuous symmetric buckles in sine form in the longitudinal direction and two lobes in the circumferential direction corresponding to the shell's shape from the first mode of Eigenvalue analysis [42].

$$a = 1 \cdot 728\sqrt{Rt} \tag{7}$$

$$w = w_0 \, sin(\pi y \, / \, 31.75) \, cos \, 2\theta \tag{8}$$

In equations (7 and 8), w_0 represents the amplitude of imperfection, *R* is the radius of the cylinder, *t* is the cylinder thickness, and *y* corresponds to the longitudinal direction, providing two lobes in the circumferential direction. Eq. (8) is parametrized and integrated into the model as an equation-driven surface [42]. In this study, 3 amplitudes of 0.005, 0.05, and 0.5 mm as axisymmetric imperfections, as described in Eq. (8), are incorporated into the geometric models. For this purpose, three nomenclatures as 0.005AI, 0.05AI, and 0.5AI are defined to investigate the effect of axisymmetric imperfections on the buckling performance of steel cylindrical shell strengthened by CFRP under combined axial compression and torsion.

3 Numerical results and discussion

Table provides a summary of all cylindrical shell models analyzed in this study. The analysis employed a sensitivity approach to investigate the influence of different parameters on the performance of the shells under combined axial and torsional loading. The models are categorized based on the type of sensitivity analysis conducted S-AT-G1 to SC-AT-CG3 explore the effect of shell thickness (1.25 mm, 0.625 mm, and 2.5 mm) on steel (S), CFRP (C), and CFRP-strengthened steel shells (SC) shells under combined axial and torsional loading (AT). SC-AT-Mss1 to SC-AT-Mtm2 investigate the influence of CFRP material properties in steel shells strengthened by CFRP. This includes variations in stacking sequence (SC-AT-Mss1 to SC-AT-Mss3) and transverse modulus (SC-AT-Mtm1 and SC-AT-Mtm2). SC-AT-AI005 to SC-AT-AI5 examine the impact of axisymmetric imperfections (0.005 mm, 0.05 mm, and 0.5 mm) on the performance of CFRP-strengthened steel shells (SC-AT).

Table 9: Summary of analyzed models.

No.	Sensitivity analysis	Models	Description
1	Geometry	S-AT-G1	Steel cylindrical shell under axial and torsional loading with a thickness of 1.25 mm
2	Geometry	S-AT-G2	Steel cylindrical shell under axial and torsional loading with a thickness of 0.625 mm
3	Geometry	S-AT-G3	Steel cylindrical shell under axial and torsional loading with a thickness of 2.5 mm
4	Geometry	C-AT-G1	CFRP cylindrical shell under axial and torsional loading with a thickness of 1.25 mm
5	Geometry	C-AT-G2	CFRP cylindrical shell under axial and torsional loading with a thickness of 0.625 mm
6	Geometry	C-AT-G3	CFRP cylindrical shell under axial and torsional loading with a thickness of 2.5 mm
7	Geometry	SC-AT-SG1	Steel cylindrical shell strengthened by CFRP both with a thickness of 1.25 mm under axial and torsional loading
8	Geometry	SC-AT-SG2	Steel cylindrical shell with a thickness of 0.625 mm strengthened by CFRP under axial and torsional loading
9	Geometry	SC-AT-SG3	Steel cylindrical shell with a thickness of 2.5 mm strengthened by CFRP under axial and torsional loading
10	Geometry	SC-AT-CG2	Steel cylindrical shell strengthened by CFRP with a thickness of 0.625 mm under axial and torsional loading
11	Geometry	SC-AT-CG3	Steel cylindrical shell strengthened by CFRP with a thickness of 2.5 mm under axial and torsional loading
12	Material	SC-AT-Mss1	Steel cylindrical shell strengthened by CFRP with 4 Stacking sequence under axial and torsional loading
13	Material	SC-AT-Mss2	Steel cylindrical shell strengthened by CFRP with 8 Stacking sequence under axial and torsional loading
14	Material	SC-AT-Mss3	Steel cylindrical shell strengthened by CFRP with 10 Stacking sequence under axial and torsional loading
15	Material	SC-AT-Mtm1	Steel cylindrical shell strengthened by CFRP with Low Transverse Modulus (-50%) under axial and torsional loading
16	Material	SC-AT-Mtm2	Steel cylindrical shell strengthened by CFRP with High Transverse Modulus (+50%) under axial and torsional loading
17	Imperfection	SC-AT-AI005	Steel cylindrical shell strengthened by CFRP with axisymmetric imperfection of 0.005 mm
18	Imperfection	SC-AT-AI05	Steel cylindrical shell strengthened by CFRP with axisymmetric imperfection of 0.05 mm

19	Imperfection	SC-AT-AI5	Steel cylindrical shell strengthened by CFRP with axisymmetric imperfection of 0.5 mm

Fig. presents the stress distribution within steel cylindrical shells ("S-AT-G1," "S-AT-G2," and "S-AT-G3") subjected to combined axial (2 mm displacement) and torsional (0.01 rad rotation) loading. The results show that "S-AT-G3" experiences the highest stress level (332.2 MPa). Fig. explores the relationship between shell deformation and loading for these samples. It analyzes axial shortening under axial load and rotation under torsional moment. The trend in Fig. suggests a possible link between increased shell thickness and improved buckling performance.

S-AT-G3 exhibits the highest axial and torsional stiffness (1409.43 kN/mm) and it can withstand the largest axial load (605.52 kN) before significant deformation, but also experiences the largest corresponding shortening (1.1920 mm) under this load. Similarly, it can handle the highest torsional load (65.01 kNm) with minimal twisting (0.0022 rad). Compared to S-AT-G1, S-AT-G3 exhibits significant enhancements in key performance areas. These include a 100.16% increase in axial stiffness, a 114.61% increase in maximum axial load, and a 99.67% increase in maximum torsional load. These findings suggest that the design modifications implemented in steel cylindrical shells, that is increasing the shell thickness from 1.25 mm to 2.5 mm, significantly improve the model's resistance to buckling under both axial and torsional loads. However, it's important to note that this improvement comes at the cost of a larger corresponding axial shortening (112.96% increase).

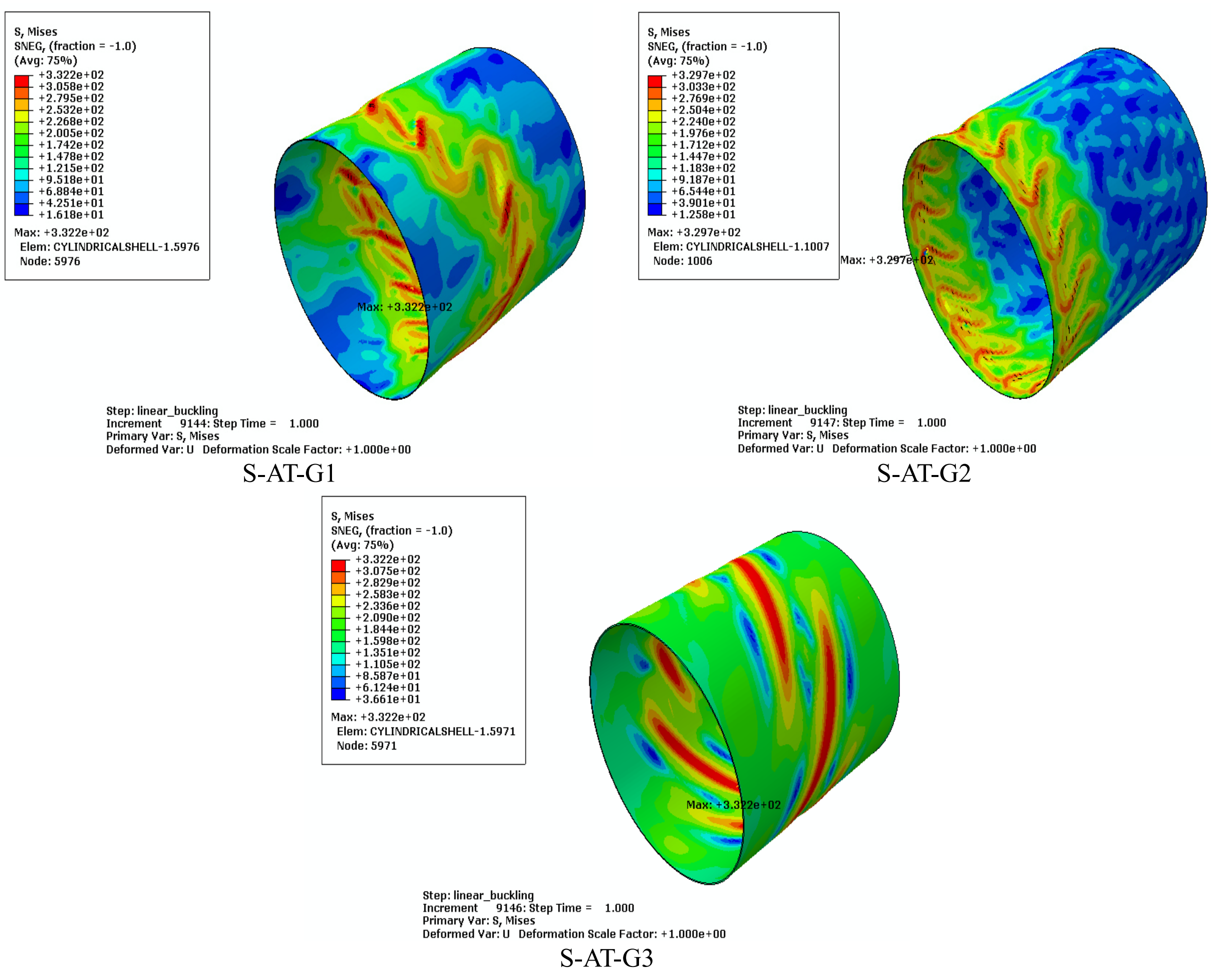

Fig. 9: Distribution of stress in steel cylindrical shells under varying thickness.

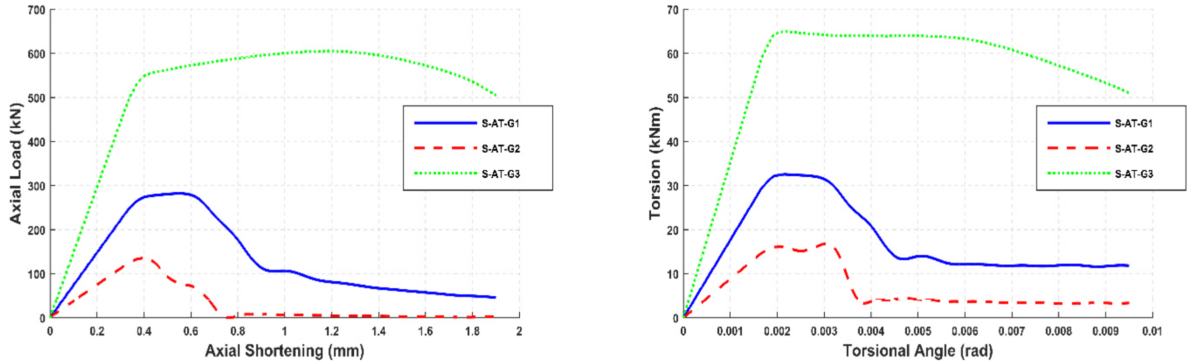

Fig. 10: Effect of shell thickness on the buckling performance of steel cylindrical shells.

Fig. presents the stress distribution within the CFRP cylindrical shells (C-AT-G1, C-AT-G2, and C-AT-G3) subjected to a combined axial load (2 mm displacement) and torsional load (0.01 rad rotation). The results indicate the highest stress level (1237 MPa) experienced by C-AT-G2 under this loading scenario.

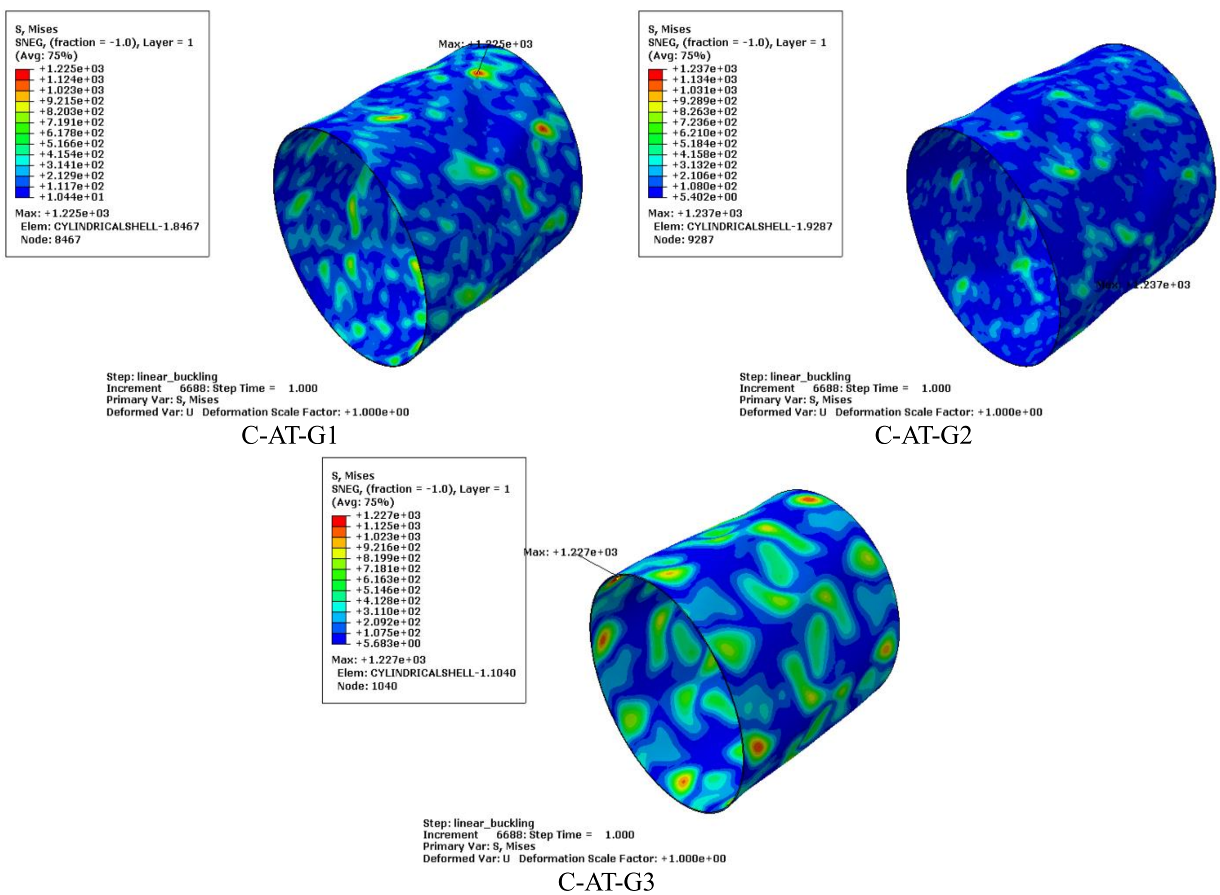

Fig. 11: Distribution of stress in CDRP cylindrical shells under varying thickness.

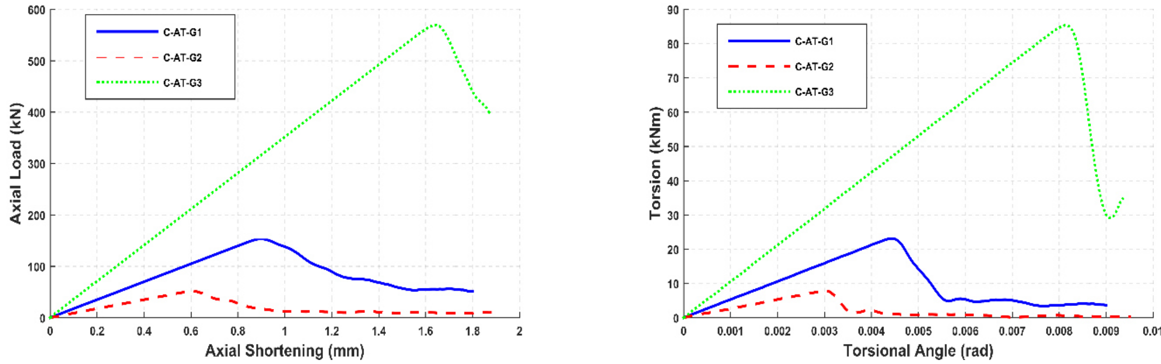

Fig. 12: Effect of shell thickness on the buckling performance of CFRP cylindrical shells.

Fig. explores the relationship between deformation and loading for these models. It analyzes axial shortening under axial load and rotation under torsional moment. The trend in Fig. suggests a link between increased shell thickness and improved buckling performance. C-AT-G3 exhibits the highest axial stiffness (358.75 kN/mm) and torsional stiffness (10624.92 kNm/rad) compared to the other models. It can also withstand the largest axial load (578.25 kN) before significant deformation. However, it experiences the largest corresponding axial shortening (1.67 mm) under this load. Similarly, it handles the highest torsional load (86.66 kNm) with minimal twisting (0.0082 rad). C-AT-G3 exhibits a 100.82% increase in axial stiffness, a 98.81% increase in torsional stiffness, a 241.04% increase in maximum axial load, and a 238.31% increase in maximum torsional load. This improved performance comes at the cost of a larger corresponding axial shortening (70.41% increase) for C-AT-G3 compared to C-AT-G1. The findings suggest that increasing the shell thickness from 1.25 mm to 2.5 mm significantly improves the CFRP cylindrical shell's resistance to buckling under combined loading. However, this improvement comes at the cost of increased axial shortening.

Fig. presents the stress distribution within the steel cylindrical shells reinforced with CFRP (SC-AT-SG1, SC-AT-SG2, and SC-AT-SG3) subjected to a combined axial load (4, 4, and 8 mm displacement respectively) and torsional load (0.02, 0.02, and 0.04 rad rotation). The results indicate the highest stress level (1913 MPa) experienced by SC-AT-SG3 under this loading scenario. Furthermore, the stress distribution of SC-AT-SG2 and SC-AT-SG3 is also shown in this figure subjected to a combined axial load (4 and 8 mm displacement respectively) and torsional load (0.02, and 0.04 rad rotation). For these two models, the highest stress level (3347 MPa) belongs to SC-AT-SG3.

Fig. explores the relationship between deformation and loading for these models. It analyzes axial shortening under axial load and rotation under torsional moment. The trend in Fig. suggests a possible link between CFRP reinforcement, improving the thickness of the steel cylindrical shell, and improved buckling performance. SC-AT-SG3 exhibits the highest overall performance among the reinforced models. It has the highest axial stiffness (1011.60 kN/mm) and torsional stiffness (23996.21 kNm/rad). It can also withstand the largest axial load (996.75 kN) before significant deformation. However, it experiences the largest corresponding axial shortening (3.96 mm) and the largest maximum torsional load (143.66 kNm) with the highest corresponding torsional angle (0.0238 rad). It also demonstrates modest improvements in axial and torsional stiffness (around 10%) compared to SC-AT-SG1. However, it exhibits significant increases in maximum axial load (75.79%) and maximum torsional load (93.70%). This suggests improved load capacity under both axial and torsional loading. The increased load capacity of SC-AT-SG3 comes at the cost of a larger corresponding axial shortening (75.23%) compared to SC-AT-SG1. It can be concluded that doubling the thickness of the steel shell reinforced with CFRP compared to the other models, contributes to its higher load capacity.

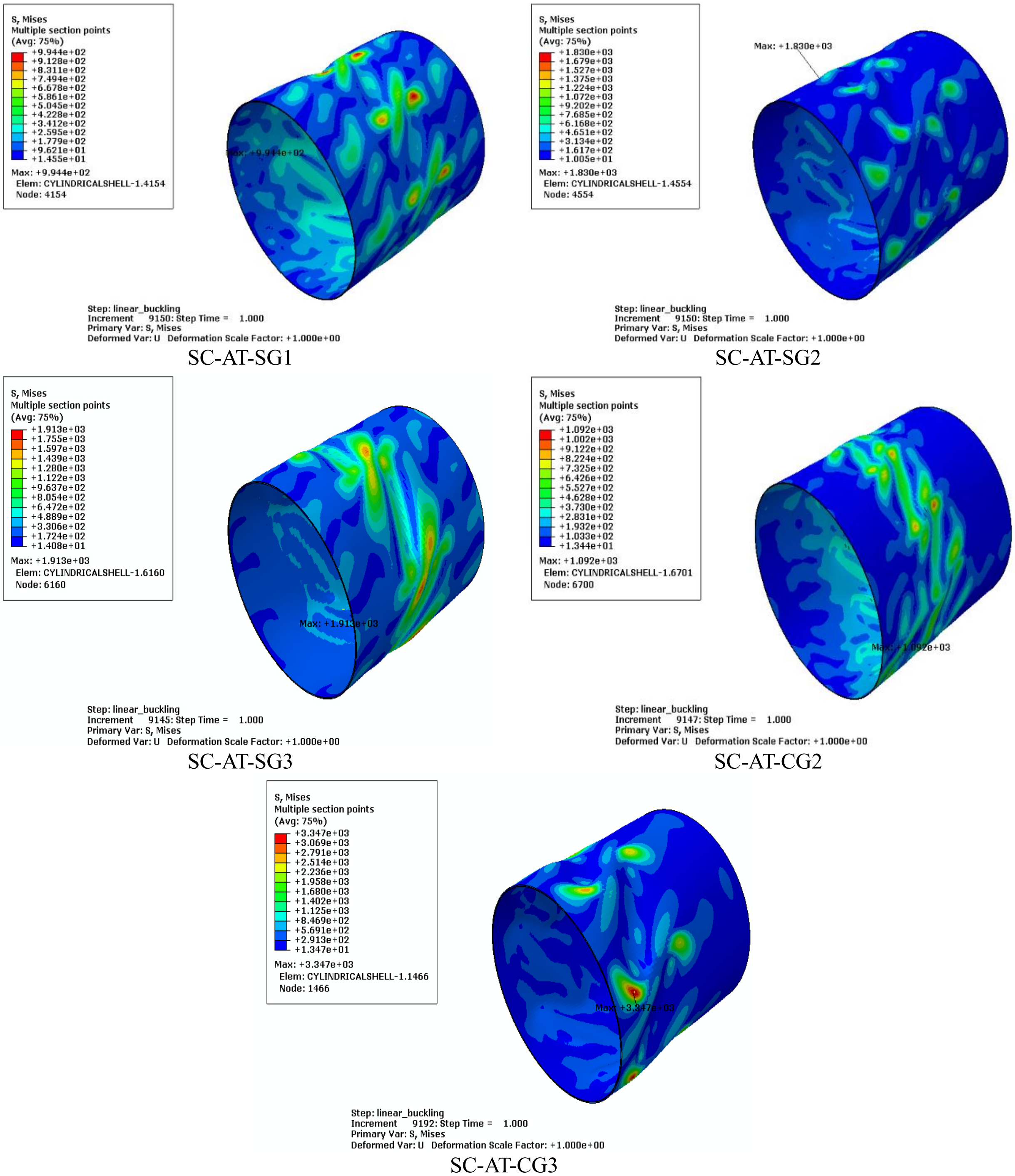

Fig. 13: Distribution of stress in CFRP-strengthened steel shells under varying thickness.

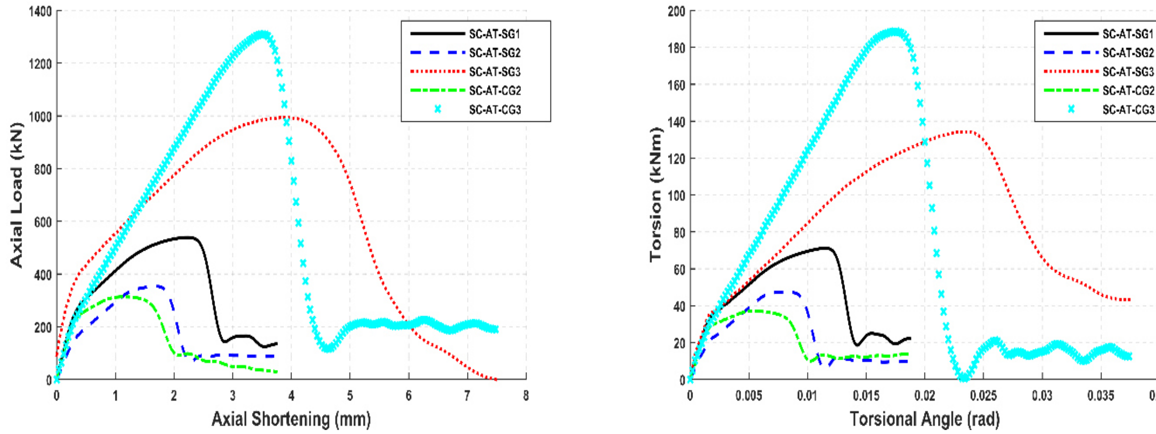

Fig. 14: Effect of shell thickness on the buckling performance of CFRP-strengthened steel shells.

The results, for SC-AT-CG2 and SC-AT-CG3 models, in which the thickness of the CFRP was doubled instead of the steel core indicates only higher amount of maximum axial and torsional loads compared to SC-AT-SG1. Thus, in such a condition, SC-AT-SG3 exhibits a significant advantage in both axial stiffness (29.5%) and torsional stiffness (24.2%) compared to SC-AT-CG3. This suggests that doubling the thickness of the steel core in SC-AT-SG3 contributes to its higher resistance to compression and twisting. Interestingly, SC-AT-CG3 demonstrates a higher maximum axial load and torsion (37.5% and 35.74% higher respectively) than SC-AT-SG3 due to the thickness doubling of the CFRP cover. Both models experience similar levels of axial shortening under maximum axial load. However, SC-AT-SG3 exhibits a larger corresponding torsional angle under the maximum torsional load compared to SC-AT-CG3. Thus, if high axial and torsional stiffness are crucial, increasing the thickness of the steel core is the better while if maximum axial load capacity is the primary concern, increasing the thickness of the CFRP cover is preferable despite its lower stiffness.

Fig. presents the stress distribution within the steel cylindrical shells reinforced with CFRP (SC-AT-Mss1, SC-AT-Mss2, and SC-AT-Mss3 with different stacking sequence and SC-AT-Mtm1 and SC-AT-Mtm2 with different transverse modulus) subjected to a combined axial load (8, 8, 8, 4, and 8 mm displacement respectively) and torsional load (0.04, 0.04, 0.04, 0.02, and 0.04 rad rotation respectively). The results indicate the highest stress level (1646 MPa) experienced by SC-AT-Mss2 under this loading scenario. Furthermore, the stress distribution of SC-AT-Mtm1 and SC-AT-Mtm2 is also shown in this figure subjected to a combined axial load in which the highest stress level (1599 MPa) belongs to SC-AT-Mtm2.

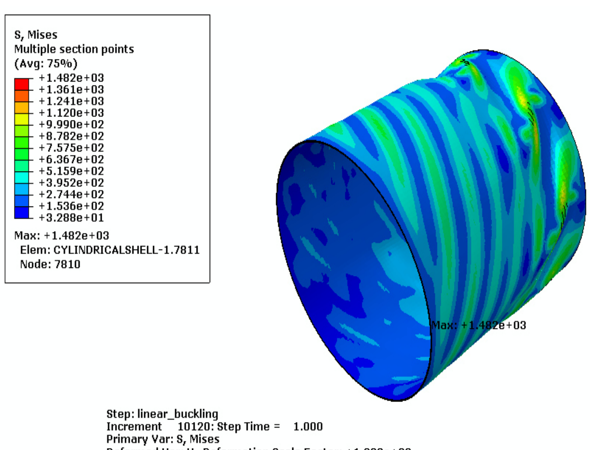

SC-AT-Mss1

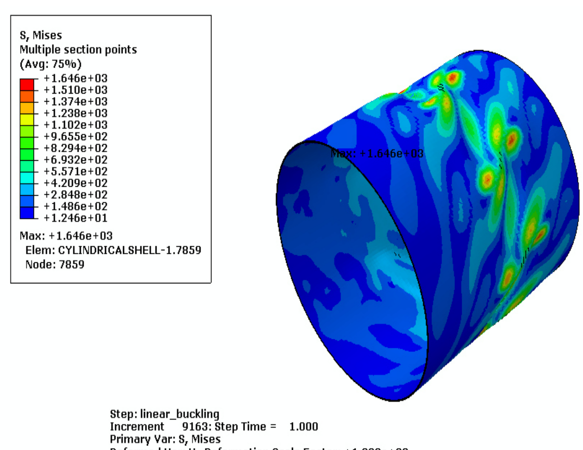

SC-AT-Mss2

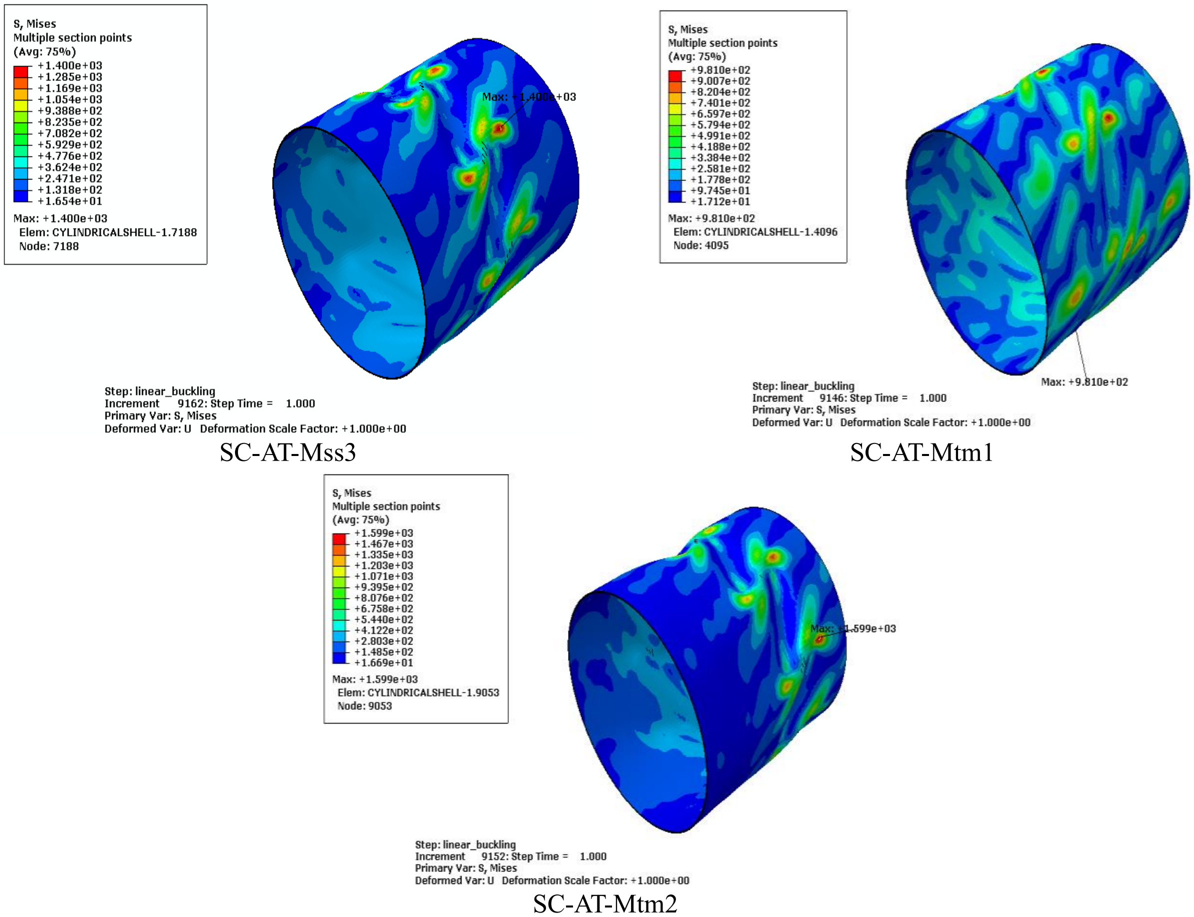

Fig. 15: Stress distribution in CFRP-strengthened steel shells under material variation.

Fig. presents the performance of two sets of steel cylindrical shells reinforced by CFRP (SC-AT-Mss and SC-AT-Mtm) under axial and torsional loading, along with a comparison to a baseline model (SC-AT-SG1). All models (SC-AT-Mss1, SC-AT-Mss2, SC-AT-Mss3, SC-AT-Mtm1, and SC-AT-Mtm2) show improvements in axial shortening, maximum torsional load, and corresponding torsional angle compared to the baseline model (SC-AT-SG1). Among these five models, SC-AT-Mss3 exhibits the highest axial and torsional stiffness among the Mss models, while SC-AT-Mtm1 has the highest for the Mtm models. It can be observed that increasing the stacking sequence increases almost the axial and torsional stiffness as well as the maximum axial and torsional load capacity while 50% increase in transverse modulus only increases the maximum axial and torsional load capacity.

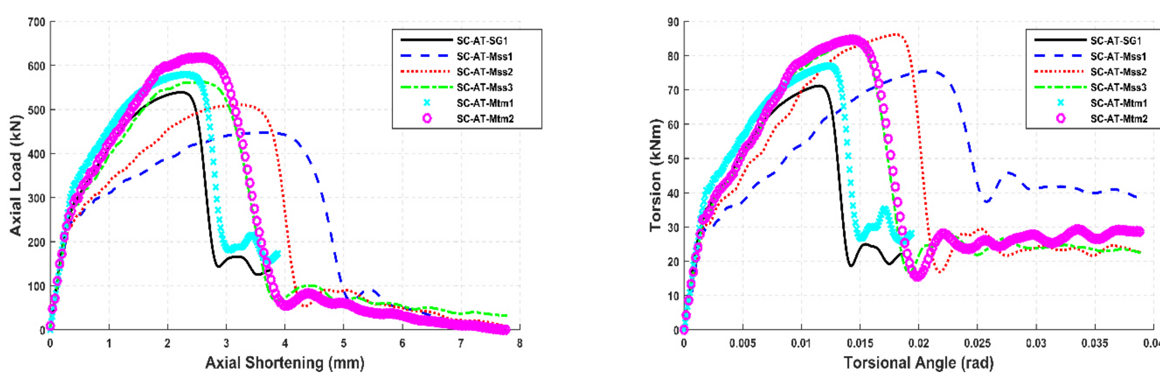

Fig. 16: Effect of material variation on the buckling performance of CFRP-strengthened steel shells.

Fig. presents the stress distribution within the steel cylindrical shells reinforced with CFRP with different axisymmetric imperfections (SC-AT-AI005, SC-AT-AI05, and SC-AT-AI5) subjected to a combined axial load (4 mm displacement) and torsional load (0.02 rad rotation). The results indicate the highest stress level (1099 MPa) experienced by SC-AT-AI5 under this loading scenario.

Fig. explores the relationship between deformation and loading for these models. It analyzes axial shortening under axial load and rotation under torsional moment. All models (SC-AT-AI005, SC-AT-AI05, and SC-AT-AI5) show similar or slightly lower axial stiffness and torsional stiffness compared to the baseline model (SC-AT-SG1). Furthermore, all three models exhibit very similar axial stiffness and torsional stiffness, with variations less than 2%. SC-AT-AI005 has the highest maximum axial load and torsional capacity among the three. Eventually, it can be concluded that increasing the amount of axisymmetric imperfection can slightly reduce the overall stiffness of the shell compared to a perfect cylinder, decrease the load capacity under axial or torsional loading, and influence the buckling behavior of the shell under combined loading.

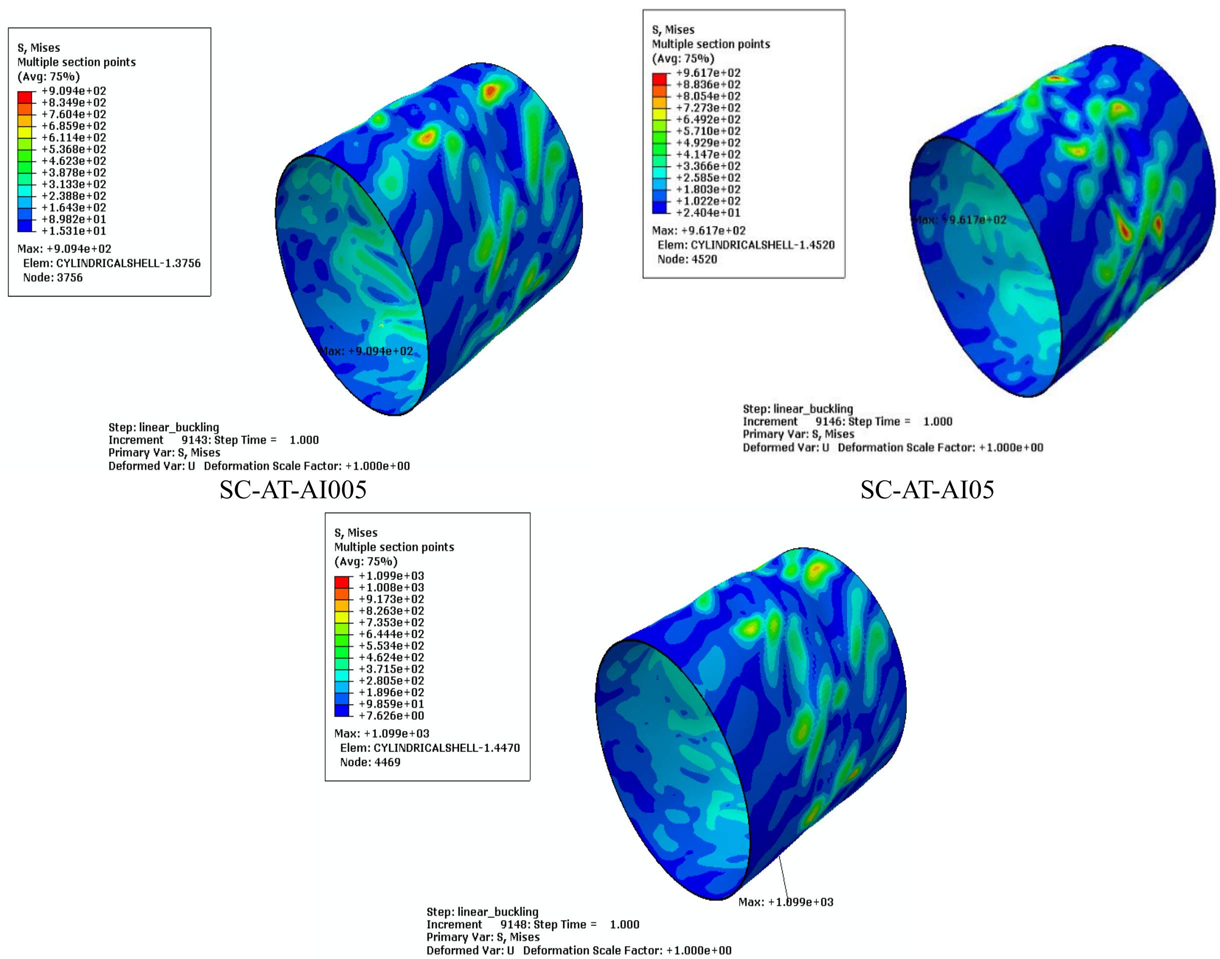

Fig. 17: Effect of axisymmetric imperfection on stress distribution in CFRP-strengthened steel shells.

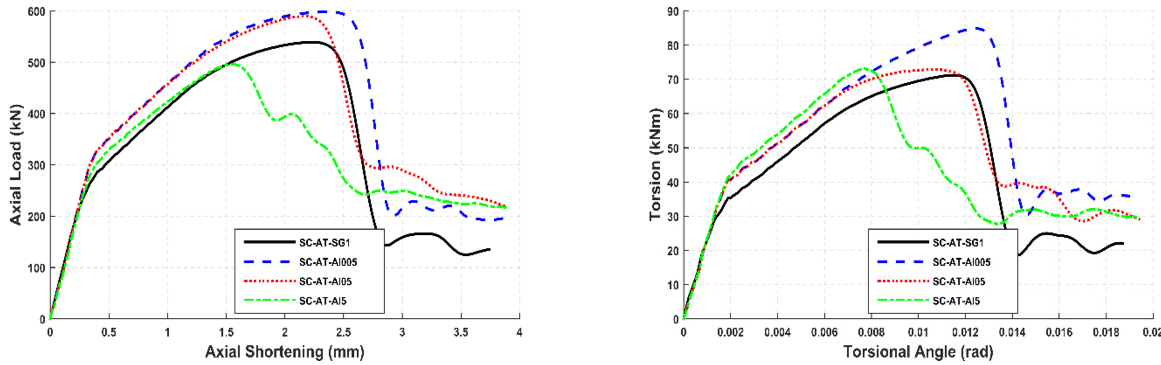

Fig. 18: Effect of axisymmetric imperfection on the buckling performance of CFRP-strengthened steel shells.

Table 9 and

Table 10 as well as Fig. summarize the buckling responses in cylindrical shells under variations in geometry, material properties, and initial imperfections.

Table 9: Detailed results of analyzed models under combined loading.

Models	Axial Stiffness [kN/mm]	Torsional Stiffness [kNm/rad]	Maximum Axial Load [kN]	Corresponding Axial Shortening [mm]	Maximum Torsional Load [kNm]	Corresponding Torsional Angle [rad]
S-AT-G1	704.1564	18111.8765	282.1571	0.5597	32.5575	0.0022
S-AT-G2	351.8740	8935.8292	135.1806	0.3968	16.8354	0.0030
S-AT-G3	1409.4322	35992.3956	605.5240	1.1920	65.0074	0.0022
C-AT-G1	178.6380	5344.3085	169.5556	0.9800	25.6166	0.0049
C-AT-G2	89.0372	2606.1850	52.2237	0.6100	7.9225	0.0030
C-AT-G3	358.7462	10624.9157	578.2451	1.6700	86.6646	0.0082
SC-AT-SG1	923.3711	22443.6090	567.0212	2.2600	74.1665	0.0117
SC-AT-SG2	547.5192	13033.9466	371.0385	1.7399	49.3041	0.0078
SC-AT-SG3	1011.6008	23996.2135	996.7519	3.9601	143.6637	0.0238
SC-AT-CG2	797.4483	19579.0422	337.4071	1.1800	39.4693	0.0054
SC-AT-CG3	780.7874	19327.0673	1371.4754	3.5999	195.0108	0.0176
SC-AT-Mss1	679.6905	16140.7706	447.3796	3.6802	75.5542	0.0206
SC-AT-Mss2	708.1841	17459.4664	532.2818	3.2002	87.9028	0.0182
SC-AT-Mss3	755.4772	18294.1533	583.4274	2.5601	86.1046	0.0146
SC-AT-Mtm1	871.9263	22026.1865	589.2992	2.3199	77.8903	0.0124
SC-AT-Mtm2	761.0697	18359.2691	629.5896	2.6401	86.3621	0.0146
SC-AT-AI005	874.0562	22087.2391	607.8306	2.3800	85.7294	0.0125
SC-AT-AI05	873.4861	22091.8597	599.3745	2.1799	73.6712	0.0108
SC-AT-AI5	822.3667	22514.4980	505.8343	1.5601	73.9580	0.0077

Table 10: Percentage change in performance parameters compared to reference models.

Models	Axial Stiffness [%]	Torsional Stiffness [%]	Maximum Axial Load [%]	Corresponding Axial Shortening [%]	Maximum Torsional Load [%]	Corresponding Torsional Angle [%]
	COMPARING TO S-AT-G1					
S-AT-G2	-50.03	-50.66	-52.09	-29.11	-48.29	39.77
S-AT-G3	100.16	98.72	114.61	112.96	99.67	-0.10
	COMPARING TO C-AT-G1					
C-AT-G2	-50.16	-51.23	-69.20	-37.75	-69.07	-38.78
C-AT-G3	100.82	98.81	241.04	70.41	238.31	67.36
	COMPARING TO SC-AT-SG1					
SC-AT-SG2	-40.70	-41.93	-34.56	-23.01	-33.52	-33.33
SC-AT-SG3	9.56	6.92	75.79	75.23	93.70	103.42
SC-AT-CG2	-13.64	-12.76	-40.49	-47.79	-46.78	-53.84
SC-AT-CG3	-15.44	-13.89	141.87	59.29	162.94	50.43
	COMPARING TO SC-AT-SG1					
SC-AT-Mss1	-26.39	-28.08	-21.10	62.84	1.87	76.08
SC-AT-Mss2	-23.30	-22.21	-6.13	41.60	18.52	55.57
SC-AT-Mss3	-18.18	-18.49	2.89	13.28	16.10	24.79
SC-AT-Mtm1	-5.57	-1.86	3.93	2.65	5.02	5.98
SC-AT-Mtm2	-17.58	-18.20	11.03	16.82	16.44	24.79
	COMPARING TO SC-AT-SG1					
SC-AT-AI005	-5.34	-1.59	7.20	5.31	15.59	6.84
SC-AT-AI05	-5.40	-1.57	5.71	-3.54	-0.67	-7.69
SC-AT-AI5	-10.94	0.32	-10.79	-30.97	-0.28	-34.18

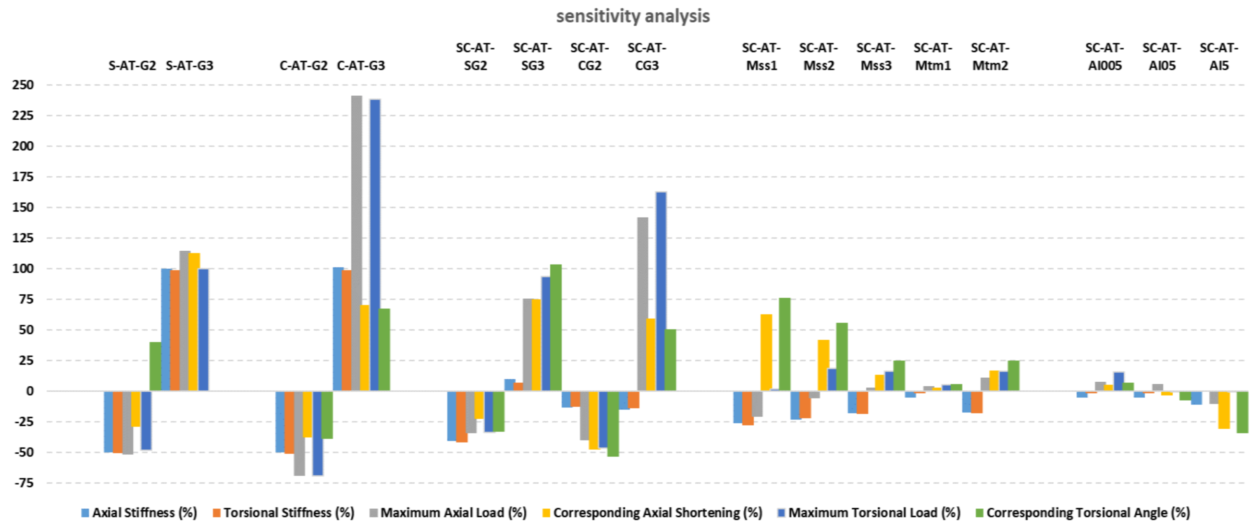

Fig. 19: Sensitivity analysis of buckling responses in cylindrical shells under variations in geometry, material properties, and initial imperfections.

Based on Table 9 and

Table 10 as well as Fig., it can be said that models with thicker shells generally exhibit increased performance compared to thinner shells, as seen in the comparisons to S-AT-G1 and C-AT-G1. Thicker shells tend to have higher load-bearing capacities and stiffness. Furthermore, models with CFRP strengthening generally show improvements in performance compared to non-strengthened counterparts, as observed in the comparisons to SC-AT-SG1. Eventually, variations in material properties and imperfections lead to mixed results. Some models show improvements while others exhibit reductions in performance compared to reference models.

The sensitivity analysis results suggest that the sensitivity of different parameters varies depending on the specific model and the design changes implemented.

• Axial stiffness and torsional stiffness seem to be highly sensitive for models with significant geometry changes (thinner shells) but show moderate sensitivity for models with minor adjustments. S-AT-G2 and C-AT-G2 show a decrease of over 50% compared to baselines due to potentially thinner shells.

• Maximum axial load can be significantly increased by using stronger materials or thicker shells but might show moderate variations for other design modifications. C-AT-G3 shows a significant increase (over 240%) compared to C-AT-G1, due to a thicker shell while SC-AT-SG3 shows a substantial increase (over 75%) compared to SC-AT-SG1, due to increased shell thickness in steel core.

• Based on these findings, the shell thickness plays a significant role in enhancing buckling performance under both axial and torsional loads. A thicker shell provides greater axial stiffness, which increases its critical buckling load and thus its resistance to axial instability. This is due to the enhanced moment of inertia and cross-sectional area, which delay the onset of axial buckling. Similarly, in torsion, increased thickness raises the polar moment of inertia, thereby improving the shell’s capacity to resist twisting deformations. As a result, a thicker shell can carry higher torsional loads before buckling as predicted by the theoretical equations presented in earlier sections. Based on this, the G3 samples with the highest thickness (2.5 mm) exhibits the highest overall performance among the models under both axial compression and torsion.

• The SC-AT-Mss3 specimen, strengthened with a 10-layer CFRP stacking sequence, exhibits the highest axial and torsion capacities due to the increased reinforcement provided by the additional CFRP layers. These extra layers significantly enhance the shell's overall stiffness, raising both the axial and torsional load capacities by increasing the moment of inertia and polar moment of inertia, which resist buckling under compressive and torsional loads.

• The improved performance of SC-AT-Mtm2 can be attributed to its higher transverse modulus, which provides increased stiffness perpendicular to the fiber direction. This enhanced stiffness allows for better load distribution and stability under axial and torsional loads, resulting in a higher critical load capacity and greater resistance to buckling. Additionally, the high transverse modulus facilitates more effective load transfer between the CFRP and steel layers, further improving the specimen's buckling resistance.

• Corresponding axial shortening generally shows a decrease for most models, indicating improved performance under axial load.

• The sensitivity of maximum torsional load and corresponding torsional angle requires more data for a conclusive analysis.

4 Conclusion

This study focused on the buckling performance of thin, circular, cylindrical shells under combined axial and torsional loading, with an emphasis on the role of CFRP reinforcement. The main objective was to explore how CFRP strengthening influences the buckling behavior of steel shells and to evaluate the effects of various parameters such as thickness, stacking sequence, and imperfections. The research methodology included reproducing reference experimental specimens, validating the FE modeling in ABAQUS against experimental and theoretical results, and conducting sensitivity analyses on steel, CFRP, and CFRP-strengthened steel shells. Key findings are summarized as follows:

• Shell Thickness: Increasing shell thickness significantly enhances axial and torsional stiffness, allowing shells to withstand higher loads before buckling. However, this improvement comes at the cost of increased axial shortening under compression.

• CFRP Reinforcement: Strengthening steel shells with CFRP notably improves buckling performance by enhancing stiffness and load capacity. The effectiveness of reinforcement depends on factors such as laminate properties, stacking sequence, and transverse modulus.

• Imperfections: Axisymmetric imperfections negatively affect buckling performance by slightly reducing stiffness and load capacity and altering the failure behavior under combined loading.

• Parameter Sensitivity: Geometric changes (e.g., thinner shells) show high sensitivity in stiffness, while maximum axial load is more responsive to material strength and thickness increases.

These findings provide valuable insights for designing cylindrical shells for aerospace and structural applications, such as aircraft fuselages and launch vehicles. Future research can investigate the influence of different fiber types, adhesives, and advanced CFRP material models incorporating non-linearity and damage mechanisms. Exploring the synergy between CFRP reinforcement and other techniques, such as stringers or ring stiffeners, could further enhance buckling performance.

References

[1] SHARIATI, M., HATAMI, H., TORABI, H., & EPAKCHI, H. R. (2012). Experimental and numerical investigations on the ratcheting characteristics of cylindrical shell under cyclic axial loading. Structural Engineering and Mechanics, 44(6), 753-762.

[2] IFAYEFUNMI, O. (2016). Buckling behavior of axially compressed cylindrical shells: Comparison of theoretical and experimental data. Thin-walled structures, 98, 558-564.

[3] WAGNER, H. N., HÜHNE, C., & JANSSEN, M. (2020). Buckling of cylindrical shells under axial compression with loading imperfections: An experimental and numerical campaign on low knockdown factors. Thin-Walled Structures, 151, 106764.

[4] TAFRESHI, A., & BAILEY, C. G. (2007). Instability of imperfect composite cylindrical shells under combined loading. Composite Structures, 80(1), 49-64.

[5] SHAHGHOLIAN-GHAHFAROKHI, D., SAFARPOUR, M., & RAHIMI, A. (2021). Torsional buckling analyses of functionally graded porous nanocomposite cylindrical shells reinforced with graphene platelets (GPLs). Mechanics Based Design of Structures and Machines, 49(1), 81-102.

[6] EKSTROM, R. E. (1963). Buckling of cylindrical shells under combined torsion and hydrostatic pressure: Tests conducted to determine the stability of thin cylindrical shells under combined loads show that the nondimensional critical hydrostatic and torsional loads, P and T, follow the parabola P+ T 2= 1. Experimental Mechanics, 3, 192-197.

[7] YAMAKI, N. (1976). Experiments on the postbuckling behavior of circular cylindrical shells under torsion. In Buckling of Structures: Symposium Cambridge/USA, June 17–21, 1974 (pp. 312-330). Berlin, Heidelberg: Springer Berlin Heidelberg.

[8] YAMAKI, N., & MATSUDA, K. (1976). Postbuckling behavior of circular cylindrical shells under torsion. Ingenieur-Archiv, 45, 79-89.

[9] DE-YU, W., HONG-WEI, M., & GUI-TONG, Y. (1992). Studies on the torsional buckling of elastic cylindrical shells. Applied Mathematics and Mechanics, 13, 211-215.

[10] LOUCA, L. A., HARDING, J. E., & LUSAS. (1994). Torsional Buckling of Ring-Stiffeners in Cylindrical Shells Subjected to External Pressure. Proceedings of the Institution of Civil Engineers-Structures and Buildings, 104(2), 219-230.

[11] TAN, D. (2000). Torsional buckling analysis of thin and thick shells of revolution. International journal of solids and structures, 37(22), 3055-3078.

[12] SOFIYEV, A. H. (2003). Torsional buckling of cross-ply laminated orthotropic composite cylindrical shells subject to dynamic loading. European Journal of Mechanics-A/Solids, 22(6), 943-951.

[13] ZHANG, L., & TONG, G. (2004). Flexural–torsional buckling of thin-walled beam members based on shell buckling theory. Thin-Walled Structures, 42(12), 1665-1687.

[14] XU, X., MA, J., LIM, C. W., & ZHANG, G. (2010). Dynamic torsional buckling of cylindrical shells. Computers & structures, 88(5-6), 322-330.

[15] XU, X., SUN, J., & LIM, C. W. (2013). Dynamic torsional buckling of cylindrical shells in Hamiltonian system. Thin-Walled Structures, 64, 23-30.

[16] NINH, D. G., BICH, D. H., & KIEN, B. H. (2015). Torsional buckling and post-buckling behavior of eccentrically stiffened functionally graded toroidal shell segments surrounded by an elastic medium. Acta Mechanica, 226(10), 3501-3519.

[17] SHAKOURI, M., SHARGHI, H., & KOUCHAKZADEH, M. A. (2017). Torsional buckling of generally laminated conical shell. Meccanica, 52, 1051-1061.

[18] CHO, H. K. (2018). Optimization of laminated composite cylindrical shells to maximize resistance to buckling and failure when subjected to axial and torsional loads. International Journal of Precision Engineering and Manufacturing, 19, 85-95.

[19] JAUNKY, N., & KNIGHT JR., N. F. (1999). An assessment of shell theories for buckling of circular cylindrical laminated composite panels loaded in axial compression. The International Journal of Solids and Structures, 36, 3799–820.

[20] FERREIRA, A. J. M., & BARBOSA, J. T. (2000). Buckling behavior of composite shells. Composite Structures, 50, 93–8.

[21] WEAVER, P. M., DRIESEN, J. R., & ROBERTS, P. (2002). The effects of flexural/twist anisotropy on compression buckling of laminated cylindrical shells. Composite Structures, 55, 195–204.

[22] ESTEKANCHI, H. E., & VAFAI, A. (1999). On the buckling of cylindrical shells with through cracks under axial load. Thin-Walled Structures, 35, 255–74.

[23] WEAVER, P. M. (2000). Design of laminated composite cylindrical shells under axial compression. Composites Part B, 31, 669–79.

[24] GEIER, B., MEYER-PEIENING, H. R., & ZIMMERMANN, R. (2002). On the influence of laminated stacking on buckling of composite cylindrical shells subjected to axial compression. Composite Structures, 55, 467–74.

[25] SUN, G., & HANSAN, J. S. (1998). Optimal design of laminated composite circular–cylindrical shells subjected to combined loads. Journal of Applied Mechanics, 55, 136–42.

[26] DIACONU, C. G., MASAKI, S., & SEKINE, H. (2002). Buckling characteristics and layup optimization of long laminated composite cylindrical shells subjected to combined loads using lamination parameters. Composite Structures, 58, 423–33.

[27] MEYER-PEIENING, H. R., FARSHAD, M., GEIER, B., & ZIMMERMANN, R. (2001). Buckling loads of CFRP composite cylinders under combined axial and torsion loading—experiments and computations. Composite Structures, 53, 427–35.

[28] SAI RAM, K. S., & SREEDHAR BABU, T. (2002). Buckling of laminated composite shells under transverse load. Composite Structures, 55, 157–68.

[29] VAZIRI, A., & ESTEKANCHI, H. E. (2006). Buckling of cracked cylindrical thin shells under combined internal pressure and axial compression. Thin-Walled Structures, 44, 141–51.
[30] STARNES JR., J. H., & ROSE, C. A. (1997). Nonlinear response of thin cylindrical shells with longitudinal cracks and subjected to internal pressure and axial compression loads. Paper no. 97-1144. AIAA.
[31] ALLAHBAKHSH, HAMIDREZA, & SHARIATI, MAHMOUD. (2012). Buckling of cracked laminated composite cylindrical shells subjected to combined loading. Applied Composite Materials.
[32] Batikha, M. (2008). Strengthening of thin metallic cylindrical shells using fiber-reinforced polymers.
[33] TENG, J. G., & HU, Y. M. (2007). Behaviour of FRP-jacketed circular steel tubes and cylindrical shells under axial compression. Construction and Building Materials, 21(4), 827-838.
[34] KRISHNA, G. V., NARAYANAMURTHY, V., & VISWANATH, C. (2021). Effectiveness of FRP strengthening on buckling characteristics of metallic cylindrical shells. Composite Structures, 262, 113653.
[35] DRAIDI, Z., BUI, T. T., LIMAM, A., TRAN, H. V., & BENNANI, A. (2018). Buckling behavior of metallic cylindrical shell structures strengthened with CFRP composite. Advances in Civil Engineering, 2018.
[36] TARAGHI, P., ZIRAKIAN, T., & KARAMPOUR, H. (2021). Parametric study on buckling stability of CFRP-strengthened cylindrical shells subjected to uniform external pressure. Thin-Walled Structures, 161, 107411.
[37] BISAGNI, C. (1998, September). Buckling tests of carbon-epoxy laminated cylindrical shells under axial compression and torsion. In XXI ICAS Congress, Melbourne (Australia).
[38] HUANG, H., ZHANG, Y., & HAN, Q. (2017). Inelastic buckling of FGM cylindrical shells subjected to combined axial and torsional loads. International Journal of Structural Stability and Dynamics, 17(09), 1771010.
[39] YADAV, K. K., & GERASIMIDIS, S. (2019). Instability of thin steel cylindrical shells under bending. Thin-Walled Structures, 137, 151-166.
[40] FAN, H. (2019). Critical buckling load prediction of axially compressed cylindrical shell based on non-destructive probing method. Thin-Walled Structures, 139, 91-104.
[41] WAGNER, H. N. R., HÜHNE, C., & ELISHAKOFF, I. (2020). Probabilistic and deterministic lower-bound design benchmarks for cylindrical shells under axial compression. Thin-Walled Structures, 146, 106451.
[42] KRISHNA, G. V., NARAYANAMURTHY, V., & VISWANATH, C. (2020). Modeling the buckling characteristics of the metal-FRP hybrid cylinder. Composite Structures, 250, 112505.